JOURNAL OF MECHANICS OF CONTINUA AND MATHEMATICAL SCIENCES
www.journalimcms.org

ISSN (Online) : 2454 -7190 Vol.-21, No.-07, July (2026) pp 161-175 ISSN (Print) 0973-8975

PERFORMANCE ANALYSIS OF SWIPT-BASED RF ENERGY HARVESTING IN DIVERSITY RECEIVER OVER TWDP FADING DISTRIBUTION WITH IMPERFECT CHANNEL ESTIMATION

Niku Borgohain[1], Bhargabjyoti Saikia[2], H. P. Mondal[3]

[1,2,3] Department of Electronics and Communication Engineering, DUIET, Dibrugarh University, Assam, India.

Email: [1]niku.borgohain008@gmail.com, [2]bjs784164@gmail.com, [3]mandal.haraprasad@gmail.com

Corresponding Author: **Bhargabjyoti Saikia**

https://doi.org/10.26782/jmcms.2026.07.00010

(Received: April 01, 2026; Revised: June 27, 2026; Accepted: July 10, 2026

Abstract

This work studies the performance of an M-branch Maximum Ratio Combining (M-MRC) diversity receiver system with RFEH (Radio Frequency Energy Harvesting Approach) under Imperfect Channel Estimation, considering the Two-Wave Diffuse Power (TWDP) fading distribution. Two key performance metrics, Average Bit Error Rate (ABER) and Outage Probability (OP), are used to evaluate the effects of Energy Harvesting (EH) and Imperfect Channel Estimation (ICE) on system performance across various modulation schemes. Power Splitting (PS) factor (β) is incorporated to derive the probability density function (PDF) of the received signal within the Simultaneous Wireless Information and Power Transfer (SWIPT) framework. Monte Carlo simulations validate the analytical expressions for ABER and OP derived from the considered PDF, highlighting the impact of EH and ICE on system performance and offering insights for optimizing wireless communication systems in fading environments. These results offer key strategies for building energy-efficient, robust wireless networks by optimizing the diversity receiver to handle harsh fading conditions.

Keywords: Energy Harvesting, SWIPT, ABER, Outage Probability, TWDP Fading, MRC Receiver, Imperfect Channel Estimation.

I. Introduction

Fading represents a significant challenge to reliable data transfer in wireless communication systems. It arises from multipath propagation, leading to signal strength fluctuations and degrading system performance. This performance degradation is a major concern for modern systems such as mobile communication, Wireless Sensor Networks (WSNs), and the Internet of Things (IoT), where energy efficiency and system reliability are essential.

In wireless communication systems, diversity techniques are extensively applied to minimize the adverse effects of fading, noise, and channel estimation errors [XXVII]. In recent studies, diversity techniques like the M-MRC receiver achieve the best Bit Error Rate (BER) and outage performance, and optimally integrate multiple received Signal-to-Noise Ratios (SNRs). It effectively improves performance in various fading environments, including Rayleigh, Nakagami-m, TWDP, $\kappa-\mu$, and Beaulieu-Xie fading distributions [VIII, XIV, XVIII]. However, as discussed in these studies, achieving optimal performance requires precise estimation of both the signal's phase and amplitude, which is highly challenging and often impractical [XVI]. Several studies [III-V,IX,XII,XVII,XXII,XXIX,XXXIII,XXXIV] have analysed the efficiency of diversity receivers, with particular focus on the impact of the channel estimation errors. In [XXIV], the impact of antenna correlation and imperfect channel estimation (ICE) on Bit Error Rate (BER) and Outage Probability (OP) is analysed, considering their combined effects on system performance.

The TWDP fading model, proposed in 2002 in [X], offers a more realistic representation of signal behaviour by incorporating two dominant specular components along with diffusely propagated wave components. This model generalizes various well-known distributions such as Rayleigh and Rician (Nakagami-n) fading. Earlier literature [XIII,XVIII,XXI,XXV] has already evaluated diversity receiver performance under TWDP fading environments, considering both perfect and imperfect channel estimation.

In modern wireless networks, SWPT has emerged as a vital technology in recent years. Even in situations where network nodes are not perfectly aligned, SWIPT enables simultaneous energy and data transmission via Radio Frequency (RF) signal [XXXI,XXXV]. The study in [XX] identifies Time-Switching-based Relaying (TSR) and Power Splitting-based Relaying (PSR) as key relaying protocols for integrating energy harvesting and information processing for SWIPT. In [XXVIII], these protocols are analysed for MIMO systems with distinct as well as co-located receivers, emphasizing the trade-off between maximum data rate and harvested energy. Additionally, [XXXVI] focuses on optimising the Secrecy Rate (SR) in mmWave IoT systems by proposing a semidefinite relaxation-based alternating optimization method for scenarios with and without ICE.

Energy harvesting, when combined with diversity techniques like MRC, enhances energy efficiency and system reliability in fading environments [VI,VII,XV,XXX,XXXII]. Reference [XXXII] derives closed-form expressions for Average Symbol Error Probability (ASEP), Outage Probability (OP), and throughput in a single-hop wireless system operating under Nakagami-m fading with perfect channel state information (CSI). The influence of energy harvesting on an L-MRC receiver in Rayleigh fading with perfect CSI was analysed in [VI] with respect to ABER and OP. Additionally, [VII] derives analytical expressions for OP and ABER in Nakagami-m fading while incorporating energy harvesting, assuming perfect CSI.

The Capacity and Outage Probability (OP) of Nonorthogonal Multiple Access (NOMA) networks with nonlinear EH and multiple-antenna users under ICE in Rayleigh Fading were analysed in [XV]. Additionally, the role of Reconfigurable Intelligent Surfaces (RIS) in RF energy harvesting systems for improving sustainability and reliability was examined in [XXX], considering imperfect CSI over Nakagami-m fading. A κ-μ fading-based two-way decode-and-forward relay network with SWIPT capability has been investigated in [XXIII]. It derives algebraic expressions for OP, throughput, and energy efficiency and validates them through simulations. In [II], a SWIPT-enabled Massive MIMO (mMIMO) system for multiuser multicell transmission, incorporating 3D mMIMO with Rician fading and nonlinear energy harvesting for enhanced practicality.

Despite extensive study into fading and EH individually, there is a lack of research examining the simultaneous impact of ICE and EH on diversity receivers. This study addresses the existing research gap by investigating the ABER and OP of an M-MRC receiver using adaptive modulation schemes (m-PSK and m-QAM) with ICE and EH under a TWDP fading environment. A PDF for EH is generated, incorporating a Power Splitting (PS) factor within the SWIPT framework, while accounting for ICE. Using this PDF, analytical expressions for ABER and OP are derived and verified through Monte Carlo simulations. The study further explores how varying numbers of receiver branches (M) affect system performance and provides useful guidelines for optimizing diversity techniques in fading environments.

The layout of this work is organized into six sections. Section 2 introduces the system and the fading channel model. Section 3 presents the derivation of the output signal PDF for an M-MRC receiver incorporating EH and ICE. Section 4 presents ABER and OP expressions for different modulation schemes. Section 5 provides numerical results and discussions, followed by conclusions in Section 6.

II. System Design

The analyzed system design model is described in Figure 1. The M-MRC receiver operates in slowly varying, frequency-nonselective flat TWDP fading. The received signal during the i^{th} symbol period is expressed by the following equation

$$\varphi(i) = \xi(i)x(i) + \nu(i) \tag{1}$$

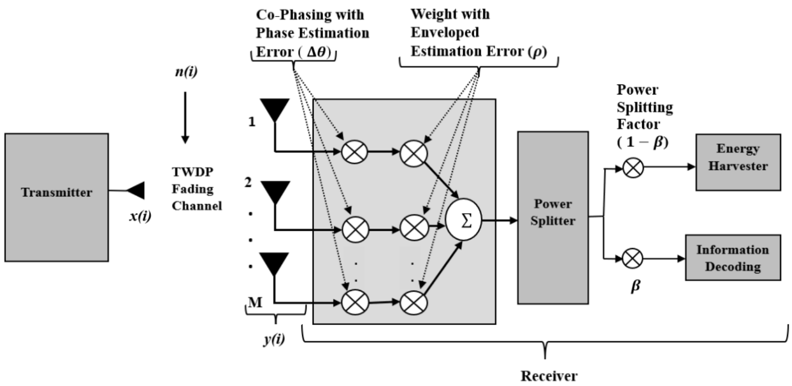

Fig. 1. Proposed System Model

The symbol *x(i)* denotes the transmitted symbol in the i^{th} period, associated with an energy of $E_x = E\left[\left|x(i)\right|^2\right]$. The complex Gaussian noise, denoted by the vector representation $\nu(i)=\left[\nu_1(i),\nu_2(i),......,\nu_M(i)\right]^T$, is characterized by a two-sided power spectral density *2N0* and a zero mean. In the specified system design, the coefficient vector of the channel for the receiver with 'M' branches is indicated as $\xi(i)=\left[\xi_1(i),\xi_2(i),.....,\xi_3(i)\right]^T$, with each component following a TWDP fading distribution. In [X], the envelope PDF corresponding to a TWDP fading channel is expressed as follows,

$$f_\xi(\xi)=\frac{\xi}{\sigma^2}\exp\left(\frac{-\xi^2}{2\sigma^2}-K\right)\sum_{i=1}^{L}a_i\Omega\left(\frac{\xi}{\sigma},K,C_i\right) \tag{2}$$

where, ξ represents the TWDP fading amplitude, $\sigma=E\left(\xi^2\right)$, $C_i=\Delta\cos\frac{\pi(i-1)}{2M-1}$, $\Omega(g,K,C_i)=1/2\left(e^{CK}I_0\left(g\sqrt{2K(1-C_i)}\right)+e^{-CK}I_0\left(g\sqrt{2K(1+C_i)}\right)\right)$, $g=\frac{\delta}{\sigma}$, Δ=convenient parameter = (peak specular power/average specular power) – 1, L denotes the order, *K*=specular power/diffused power, and 'a_i' is a constant as stated in [X]. Let $\hat{\xi}(i)=\left[\hat{\xi}_1(i),\hat{\xi}_2(i)........,\hat{\xi}_M(i)\right]^T$ represents the receiver-side channel estimation vector. The channel estimation error (CEE) at each branch can be denoted as $e_l(i)=\hat{\xi}_1(i)-\xi_l(i)$. A comprehensive framework for the ICE of any random linear channel estimation (CE) is given as [XVI],

$$\xi_{w,t}(i)=\rho_t\hat{\xi}_{w,t}(i)+z_{w,t}(i) \tag{3}$$

In Eq. (3), t = 1, 2, 3,…, M, 'w' denotes the diffused multipath components, and $\left\{z_{w,t}(i)\right\}_{t=1}^{M}$ represents the i.i.d. (independent identically distributed) estimation error with a mean of 'zero' and variance of σ_z^2. ρ_t is the normalized estimation correlation coefficient between $\xi_t(i)$ and $\hat{\xi}_t(i)$, expressed as $\rho_t=|\rho_t|e^{j\Delta\theta_t}$. Here, $\Delta\theta_t$ is denoted as the phase offset of ρ_t. In case of imperfect channel estimation, the receiver's performance is compromised in the occurrence of $|\rho_t|<1$ or $\Delta\theta_t\neq 0$ or both [XVI].

The signal from the M-MRC receiver output is transmitted into a power splitter module. In an ideal scenario, this signal is considered to be noise-free. The power splitter distributes the signal's energy into two components: one used for information decoding (ID) with a power factor of β, and the other for energy harvesting with a splitting factor of $1-\beta$. The power splitter factor β, has a range of 0 to 1 and can be adjusted for varied fading situations. The signals are divided between the ID receiver, which performs various standard functions, and the energy harvesting receiver, which captures a portion of the energy [VI, VII].

Output SNR Incorporating ICE:

For the detection of the symbol $x(i)$, ICE requires a complex DV (Decision Variable), which may be represented as $\widehat{D} = \sum_{t=1}^{M} \hat{\xi}_t(i) y_t(i)$, where M denotes the number of receive antennas. By utilizing the half-plane decision (HPD) method, a new decision variable is obtained in which the complicated decision variable $\widehat{D}$ undergoes a rotation by an angle ψ, as described in [XVI],

$$D(\psi) = \Re\left(\widehat{D} e^{-j\psi}\right) \tag{4}$$

with $\psi = \pm\left(\frac{\pi}{2} - \frac{\pi}{N}\right)$ and where 'N' represents the constellation size. The corresponding output SNR of the MRC receiver with the half plane decision (HPD) method for a DV 'D', is formulated as [XVI]

$$\gamma_{ICE}^{MRC} = B(\psi) \sum_{t=1}^{M} \hat{\gamma}_t \tag{5}$$

Here, B is derived as a function of ψ, where $B(\psi) = \frac{|\rho_t|^2 \cos^2(\Delta\theta_t - \psi)}{\left[\left(1 - |\rho_t|^2\right)\bar{\gamma}_t + 1\right]}$, $\hat{\gamma}_t = \left|\hat{\xi}_t\right|^2 / N_0$

PDF Derivation Incorporating ICE and EH:

In an MRC combiner, the signals from all diversity receiver branches are co-phased, weighted proportionally, and combined to improve the receiver's output signal quality. The corresponding output SNR is expressed as [XXVII],

$$\gamma_{MRC} = \sum_{t=1}^{M} \gamma_t = \frac{E_b}{N_0}\left(\xi_1^{\,2} + \xi_2^{\,2} + \ldots\ldots + \xi_M^{\,2}\right) \tag{6}$$

where $\gamma_t = \left(E_b / N_0\right) \xi_t^2$ is the SNR of the t^{th} MRC receiver branch. The average output SNR is denoted by $\bar{\gamma}_t$ while the energy per bit is represented by E_b. Assuming uniform average output SNR across all branches of the receiver, the SNR PDF for each branch can be expressed for the TWDP fading as [XXV],

$$f_{\hat{\gamma}_t}(\hat{\gamma}_t) = \frac{\eta}{2B} \sum_{i=1}^{L} \sum_{j=0}^{1} a_i e^{-\{\eta\beta^{-1}B^{-1}\hat{\gamma}_t + p_{2i-j}\}} I_0\left(2\sqrt{p_{2i-j}\eta B^{-1}\hat{\gamma}_t}\right) \tag{7}$$

Following the analytical framework reported in [XXV], the output SNR PDF of the TWDP fading channel under imperfect channel estimation is adopted in this work, where the degradation due to channel estimation errors is represented through the parameter **B** derived from the estimation model in [XVI].

Here, 'B' signifies the estimation error of the receiver, I_0 represents the 0th-order Bessel Function, $\eta = \frac{K+1}{\bar{\gamma}}, p_{2i-j} = K\left[1+(-1)^j \Delta Cos\frac{\pi(i-1)}{2M-1}\right]$ and $\hat{\gamma}$ signify the SNR of the received signal with ICE. Subsequently, by implementing the random variable multiplication of the power splitter factor β at (7), denoted as $f_{\gamma_{t_{MRC}}}(\gamma_t) = \frac{1}{\beta} f_{\gamma_{t_{MRC}}}\left(\frac{\gamma_t}{\beta}\right)$, the PDF of the output SNR for each branch can be determined as,

$$f_{\hat{\gamma}_t}(\hat{\gamma}_t) = \frac{\eta}{2\beta B}\sum_{i=1}^{L}\sum_{j=0}^{1} a_i e^{-\{\eta\beta^{-1}B^{-1}\hat{\gamma}_t + p_{2i-j}\}} I_0\left(2\sqrt{p_{2i-j}\eta\beta^{-1}B^{-1}\hat{\gamma}_t}\right) \tag{8}$$

A characteristic function-based approach is employed to determine the output SNR of the M-MRC receiver. Employing the formula $\Phi_{\gamma_t}(j\omega) = \int_0^\infty e^{-j\omega\gamma_t} f_{\gamma_t}(\gamma_t)\, d\gamma_t$, the characteristic function of (8) for an individual branch can be expressed as,

$$\phi_{\gamma_t}(j\omega) = \frac{\eta}{2\beta B}\sum_{i=1}^{L}\sum_{j=0}^{1} a_i e^{-p_{2i-j}} \frac{1}{(\eta\beta^{-1}B^{-1} + j\omega)} e^{\frac{4p_{2i-j}\eta\beta^{-1}B^{-1}}{4(\eta\beta^{-1}B^{-1}+j\omega)}} \tag{9}$$

The joint characteristic function (CF) of the input SNR for an M-MRC receiver is determined by multiplying $\phi_{\gamma_t}(j\omega)$ in equation (9) as,

$$\phi_{\gamma_1....\gamma_M}(j\omega_1,......., j\omega_M) = \prod_{t=1}^{M}\left\{\frac{\eta}{2\beta B}\sum_{i=1}^{L}\sum_{j=0}^{1} a_i e^{-p_{2i-j}} \frac{1}{(\eta\beta^{-1}B^{-1} + j\omega_t)} e^{\frac{p_{2i-j}\eta\beta^{-1}B^{-1}}{(\eta\beta^{-1}B^{-1}+j\omega_t)}}\right\} \tag{10}$$

The characteristic-function expansion follows the convergent TWDP series representation reported in [X], and the subsequent analytical evaluation is performed using the standard integral identities given in [XI].

So, now, considering $\omega_1 = \omega_2 ... = \omega_M = \omega$ and expressing (10) in the form of an infinite series, from which the characteristic function (CF) is derived as,

$$\phi_{\gamma_1....\gamma_M}(j\omega_1,......., j\omega_M) =$$

$$\left(\frac{\eta}{2\beta B}\right)^M \sum_{i_1=1}^{L}...\sum_{i_M=1}^{L}\sum_{j_1=0}^{1}...\sum_{j_M=0}^{1}\sum_{s=0}^{\infty} \frac{\left\{\prod_{t=1}^{M} a_{i_t}\right\} e^{-\sum_{t=1}^{M} p_{2i_t-j_t}} \left(\sum_{t=1}^{M} p_{2i_t-j_t}\eta\beta^{-1}B^{-1}\right)^s}{s!(\eta\beta^{-1}B^{-1}+j\omega)^{M+s}} \quad (11)$$

The Probability Density Function (PDF) of the output SNR for the considered M-MRC receiver is evaluated via the inverse Fourier Transform (FT) of (11). Using the identity in [XI, (3.382.7)], and expressing the result in terms of the Hypergeometric function ${}_0F_1$, the PDFs obtained as

$$f_{\hat{\gamma}}(\hat{\gamma}) = \left(\frac{\eta}{2\beta B}\right)^M \sum_{i_1=1}^{L}...\sum_{i_M=1}^{L}\sum_{j_1=0}^{1}...\sum_{j_M=0}^{1}$$

$$\frac{\left\{\prod_{t=1}^{M} a_{i_t}\right\} e^{-\sum_{t=1}^{M} p_{2i_t-j_t}} \hat{\gamma}^{M-1} e^{-\eta\beta^{-1}B^{-1}\hat{\gamma}}}{\Gamma(M)} {}_0F_1\left(;M;\hat{\gamma}\sum_{t=1}^{M} p_{2i_t-j_t}\eta\beta^{-1}B^{-1}\right) \quad (12)$$

It is observed that when $|\rho_t| = 1$ or $\Delta\theta_t = 0$, the parameter $'B'$ approaches unity, and the modified SNR PDF reduces to the conventional TWDP fading PDF corresponding to perfect channel estimation [XXV].

III. ABER Evaluation Incorporating EH & ICE:

The ABER is obtained by substituting (12) into the corresponding ABER expression, as presented in [XXVII]. The equation is,

$$P_e = \int_0^{\infty} P(e/\hat{\gamma}) f_{\hat{\gamma}}(\hat{\gamma}) d\hat{\gamma} \quad (13)$$

where, $P(e/\hat{\gamma})$ signifies a conditional Bit Error Rate (BER). For coherent binary modulation, it is expressed as shown in [I],

$$P(e/\hat{\gamma}) = bQ\left(\sqrt{2c\hat{\gamma}}\right) \quad (14)$$

Here, the variables 'b' and 'c' denote the coherent m-ary modulations, whereas $'\tilde{m}'$ signifies the constellation size. By putting equations (12) and (14) into equation (13) and solving it with reference to [XI, p.6.455(1)], the final expression for ABER has been derived as follows:

$$P_{e,coh} = \frac{\beta^{-M} B^{-M} \eta^{M}}{2\sqrt{\pi}} \sum_{i_1=1}^{L} \cdots \sum_{i_M=1}^{L} \sum_{j_1=0}^{1} \cdots \sum_{j_M=0}^{1} \sum_{s=0}^{\infty}$$

$$\frac{\left\{\prod_{t=1}^{M} b_{i_t}\right\} b e^{-\sum_{t=1}^{M} p_{2i_t - j_t}} \left(2\sum_{t=1}^{M} p_{2i_t - j_t} \eta \beta^{-1} B^{-1}\right)^{s}}{\Gamma(M) s! (M)_s} \frac{\sqrt{c}\,\Gamma(M+s+\frac{1}{2})}{(M+s)\left(c+2\eta\beta^{-1}B^{-1}\right)^{M+s+\frac{1}{2}}}$$

$${}_2F_1\left(1, M+s+\tfrac{1}{2}; M+s+1; \frac{2\eta\beta^{-1}B^{-1}}{c+2\eta\beta^{-1}B^{-1}}\right) \tag{15}$$

Table 1: Coherent m-ary modulations ‘b’ and ‘c’ values [XXV]:

c	b		
-	1/2	1	$4\left(\sqrt{m}-1\right)/\sqrt{m}$
1	BFSK	-	-
2	-	BPSK	-
$2\sin^2\left(\pi/m\right)$	-	m-PSK	-
$3/m-1$	-	-	m-QAM

IV. Evaluation of OP incorporating EH & ICE

The Outage Probability (OP) for the considered system is obtained by substituting (12) into the OP equation provided in [XXIV], as

$$P_{out} = \int_{0}^{\gamma_{th}} f_{\hat{\gamma}}(\hat{\gamma}) d\hat{\gamma} \tag{16}$$

where, γ_{th} indicates the SNR threshold. Substituting equation (12) into (16) and evaluating the expression using the approach in [XI, 3.381.1] yields the final expression of the Outage Probability (OP) as:

$$P_{out} = \left(\frac{\eta}{2\beta B}\right)^{M} \sum_{i_1=1}^{L} \cdots \sum_{i_M=1}^{L} \sum_{j_1=0}^{1} \cdots \sum_{j_M=0}^{1} \sum_{s=0}^{\infty}$$

$$\frac{\left\{\prod_{t=1}^{M} a_{i_t}\right\} e^{-\sum_{t=1}^{M} p_{2i_t - j_t}} \left(\sum_{t=1}^{M} p_{2i_t - j_t} \eta \beta^{-1} B^{-1}\right)^{s}}{\Gamma(M) M_s s!}$$

$$\left(\eta\beta^{-1}B^{-1}\right)^{-(s+M)} g\left((s+M), \gamma_{th}\eta\beta^{-1}B^{-1}\right) \tag{17}$$

V. Numerical Results Analysis and Discussion

This section provides a complete evaluation of an M-MRC receiver over a TWDP fading environment with ICE. Numerical analysis illustrates how factors such as the power splitting parameter (β), the ICE parameters (ρ and θ), digital modulations (e.g., m-QAM and m-PSK), and diversity order (M), influence ABER and OP. The ABER is calculated using equation (15), which offers critical insights into its performance.

Figure 2 shows the ABER variation with average SNR for different parameter values β, ρ and θ. The results are obtained for M = 2 diversity branches under the TWDP fading model, characterized by fading parameters K = 3 & Δ = 0.5 for both 4-QAM and 8-QAM modulation schemes. It can be observed that for a given m-QAM modulation scheme (4-QAM or 8-QAM), the ABER decreases as β increases. While the 8 - QAM scheme exhibits a higher ABER than 4-QAM, a notable improvement in ABER is observed at β = 0.4. The presence of imperfect channel estimation (ICE) also exhibits similar behavior. A significant performance degradation is noted under ICE (ρ=0.980, θ=0^0) when compared with perfect channel estimation (ρ=1, θ =0^0). However, an increase in β significantly reduces the ABER, indicating enhanced system performance. Furthermore, at higher SNR values, the ABER improves substantially.

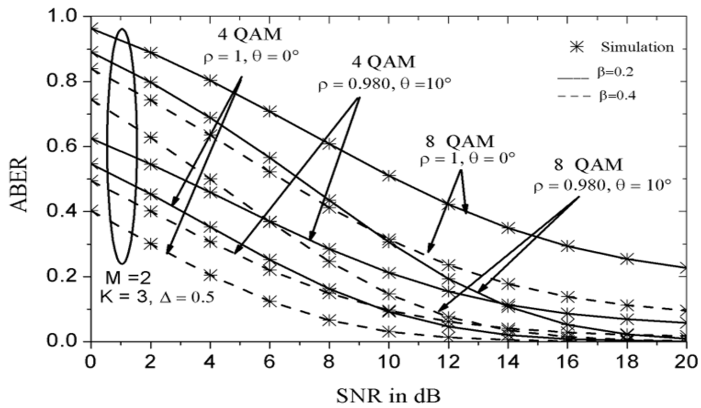

Fig. 2. Plot for ABER Evaluation with m-QAM, EH & ICE

Similarly, A comparison of ABER performance against average SNR for m-QAM and m-PSK schemes with constellation sizes of 4 and 8 is shown in Figures 3 and 4, for different values of β. The results are obtained for diversity orders M=2 and M=3 under the ICE condition over TWDP fading parameters K=3 & Δ=0.5. As shown in these plots, for both scenarios, an increasing number of receiving antennas and higher values of the β result in a remarkable improvement in system performance.

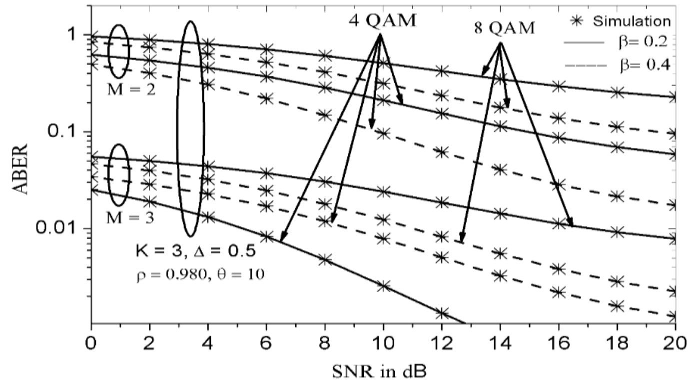

Fig. 3. ABER evaluation plot considering m-QAM, EH & ICE for different receiving branches

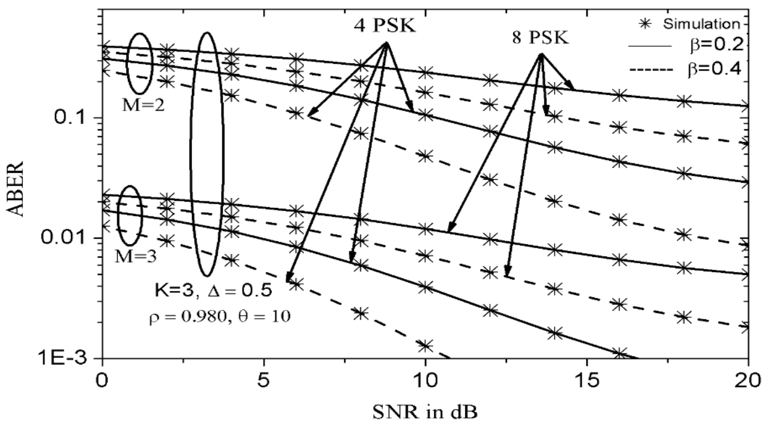

Fig. 4. Plot for ABER analysis with m-PSK, EH & ICE for different receiving branches

Figure 5 presents a comparative analysis of m-QAM and m-PSK modulation, highlighting the effect of β on ABER under ICE conditions. The plot clearly shows that at lower SNR values, m-PSK modulation (e.g., 4-PSK and 8-PSK) outperforms m-QAM modulation. As β increases, the ABER performance of M-QAM modulation improves, even at lower average SNR values. Additionally, at higher SNR and larger values of β, the ABER of an MRC receiver decreases significantly.

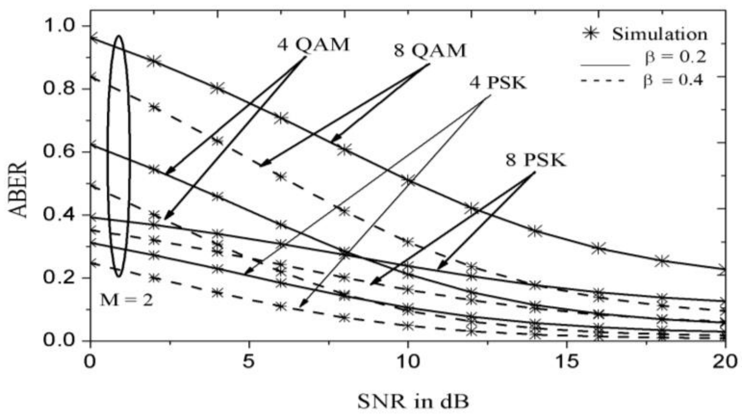

Fig. 5. Comparison plot of m-QAM & m-PSK with EH & ICE considering M=2 & K=3, Δ=0.5

In Figure 6, the ABER performance of the M-MRC receiver is evaluated under the influence of β and the TWDP fading parameters. The plot reveals that, as predicted, an increase in the 'K' parameter results in a slight decrease in ABER, while an increase in 'Δ' leads to a rise in ABER. Notably, a higher value of β significantly improves system performance under both TWDP fading scenarios.

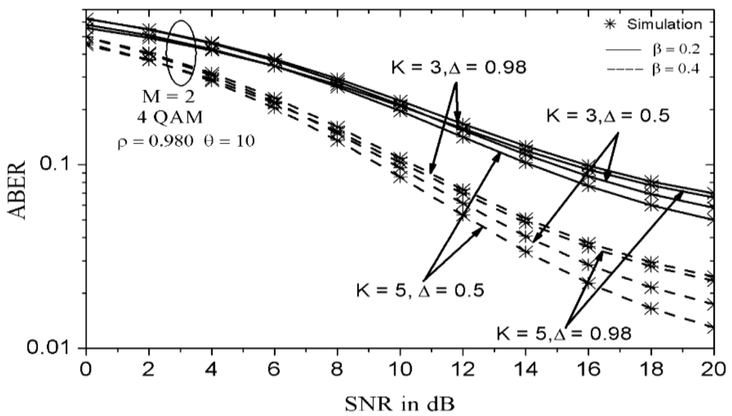

Fig. 6. Plot for ABER Evaluation for different K & Δ with EH & ICE

Figure 7 presents the outage probability of the considered system, derived using Equation 17 with a threshold SNR γ^{th} =2 dB. The plot compares the performance of two diversity branches (M=2 and *M*=3) by investigating the influence of the power-splitting factor β under ICE conditions in a TWDP fading environment. Results indicate that the system's outage probability increases under ICE conditions compared to scenarios with perfect CSI. However, increasing the β significantly improves the outage performance. Combining a higher-order diversity receiver with a larger value of β reduces the system's outage probability under TWDP fading conditions.

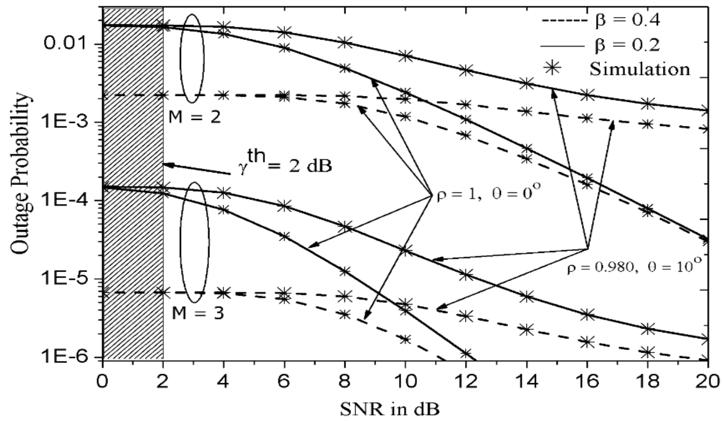

Fig. 7. Outage Probability analysis plot considering M=2 & 3, K=3, Δ=0.5

VI. Conclusions

This study analyses the ABER and OP of an M-MRC diversity receiver operating in TWDP fading channels, incorporating energy harvesting and adaptive modulation schemes under the influence of ICE. For the proposed model, the output SNR PDF was derived and used to analyze the influence of the power-splitting factor, ICE, and diversity on the system performance. The results indicated that increasing receiver branches and optimal power-splitting factor selection improved system reliability by reducing ABER and outage probability. Additionally, the performance of the receiver in adaptive modulation schemes is highly dependent on the power-splitting factor. These findings contribute to the design of robust wireless systems under TWDP fading conditions. In addition, Monte Carlo simulations were used to validate the analytical results, highlighting the effectiveness of the proposed method.

Conflict of Interest:

There was no conflict of interest regarding this paper.

References

I. Aalo, V.A., 1995. Performance of maximal-ratio diversity systems in a correlated Nakagami-fading environment. IEEE Transactions on Communications, 43(8), pp. 2360–2369. 10.1109/26.403769.

II. Adeli, M.H., Abbasi-Moghadam, D., Fotouhi, H. & Razavizadeh, S.M., 2025. Optimizing Energy Efficiency in UPA-Assisted SWIPT Massive MIMO Systems Over Rician Fading Channels. IEEE Open Journal of the Computer Society. Available at: 10.1109/OJCS.2025.3525519.

III. Aruna, G., 2015. Methodology of analysis of L-branch equal gain combiner with carrier phase error and CCI over Nakagami-m fading. International Conference on Computing and Network Communications (CoCoNet), pp. 505–510. 10.1109/CoCoNet.2015.7411233.

IV. Aruna, G. & Sahu, P.R., 2014. Performance analysis of MRC receiver with channel estimation error and CCI in Nakagami-m fading channel. Computational Intelligence and Computing Research (ICCIC), pp. 1–4. 10.1109/ICCIC.2014.7238299.

V. Badarneh, O. & Almehmadi, F.S., 2016. Performance analysis of L-branch MRC over generalized fading channels with imperfect channel estimation. IET Communications, 10(10), pp. 1175–1182. 10.1049/iet-com.2015.1015.

VI. Deka, N. & Subadar, R., 2023. Energy harvesting techniques and performance analysis for L-MRC receiver in Rayleigh fading channels. CSIT, 11, pp. 157–161. 10.1007/s40012-023-00385-y.

VII. Deka, N. & Subadar, R., 2024. Energy harvesting-based performance analysis in Nakagami-m fading channels. International Journal of Autonomous and Adaptive Communications Systems, 17(1), pp. 89–97. 10.1504/IJAACS.2024.135940.

VIII. Devi, L.M. & Singh, A.D., 2022. Channel capacity analysis of various adaptive transmission schemes and BER performance at Beaulieu-Xie fading. Radioelectronics and Communications Systems, 65, pp. 18–26. 10.3103/S0735272722010034.

IX. Duong, T.Q., Shin, H. & Hong, E.K., 2007. Error probability of binary and M-ary signals with spatial diversity in Nakagami-q (Hoyt) fading channels. EURASIP Journal on Wireless Communication and Networking, 4, pp. 1–8. 10.1155/2007/53742.

X. Durgin, G.D. & Rappaport, T.S., 2002. New analytical models and probability density function for fading in wireless communication. IEEE Transactions on Communication, 50(6), pp. 1005–1015. 10.1109/TCOMM.2002.1010620.

XI. Gradshteyn, I.S. & Ryzhik, I.M., 2007. Tables of Integrals, Series and Products. Elsevier Inc., USA.

XII. Jeong, W., Lee, J. & Yoon, D., 2011. New BER expression of MPSK. IEEE Transactions on Vehicular Technology, 60(4), pp. 1916–1924. 10.1109/TVT.2011.2114903.

XIII. Kim, D., Lee, H. & Kang, J., 2018. Comprehensive analysis of the impact of TWDP fading on the achievable error rate performance of BPSK signaling. IEICE Transactions on Communications, E101-B(2), pp. 500–507. 10.1587/transcom.2017EBP3108.

XIV. Kumar, P. & Sahu, P.R., 2014. Analysis of M-PSK with MRC receiver over κ−μ fading channels with outdated CSI. IEEE Wireless Communications Letters, 3(6), pp. 557–560. 10.1109/LWC.2014.2355849.

XV. Le-Thanh, T. & Ho-Van, K., 2024. MIMO NOMA with nonlinear energy harvesting and imperfect channel information. Arabian Journal for Science and Engineering, 49, pp. 6675–6693. 10.1007/s13369-023-08401-8.

XVI. Ma, Y., Schober, R. & Pasupathy, S., 2005. Effect of channel estimation error on MRC diversity in Rician fading channels. IEEE Transactions on Vehicular Technology, 54(6), pp. 2137–2142. 10.1109/TVT.2005.853454.

XVII. Ma, Y., Schober, R. & Pasupathy, S., 2005. Performance of M-PSK with GSC and EGC with Gaussian weighting errors. IEEE Transactions on Vehicular Technology, 54, pp. 149–162. 10.1109/TVT.2004.839674.

XVIII. Maric, A. & Njemcevic, P., 2024. Performance analysis of M-ary RQAM and M-ary DPSK receivers over the channels with TWDP fading. Wireless Networks, 30(12), pp. 3337–3347. 10.1007/s11276-024-03723-3.

XIX. Mishra, D. et al., 2015. Smart RF energy harvesting communications: challenges and opportunities. IEEE Communications Magazine, 53(4), pp. 70–78. 10.1109/MCOM.2015.7081078.

XX. Nasir, A.A. et al., 2013. Relaying protocols for wireless energy harvesting and information processing. IEEE Transactions on Wireless Communications, 12(7), pp. 3622–3636. 10.1109/TWC.2013.062413.122042.

XXI. Patangia, P.M. & Subadar, R., 2022. L-SC receiver over equally correlated TWDP channels. AEU - International Journal of Electronics and Communications, 149, p. 154173. 10.1016/j.aeue.2022.154173.

XXII. Radaydeh, R.M., 2007. Average error performance of M-ary modulation schemes in Nakagami-q (Hoyt) fading channels. IEEE Communications Letters, 11(3), pp. 255–257. 10.1109/LCOMM.2007.061323.

XXIII. Sahoo, S. & Kumar, N., 2025. Performance analysis of SWIPT-enabled two-way decode-and-forward relay network under kappa-miu fading. Annals of Telecommunications. 10.1007/s12243-025-01079-z.

XXIV. Saikia, B. & Subadar, R., 2018. Effect of estimation error on dual MRC receiver over Hoyt fading channels. International Journal of Electronics Letters. 10.1080/21681724.2018.1523470.

XXV. Saikia, B. & Subadar, R., 2019. Adaptive M-MRC scheme with estimation error over TWDP fading. International Journal of Autonomous and Adaptive Communications Systems, 12(1). 10.1504/IJAACS.2019.096668.

XXVI. Shaikh, F.K. & Zeadally, S., 2016. Energy harvesting in wireless sensor networks: A comprehensive review. Renewable and Sustainable Energy Reviews, 55, pp. 1041–1054. 10.1016/j.rser.2015.11.010.

XXVII. Simon, M.K. & Alouini, M.S., 2005. Digital Communication over Fading Channels, 2nd ed. John Wiley & Sons, Inc. 10.1002/0471715220.

XXVIII. Song, C. et al., 2014. MIMO broadcasting for simultaneous wireless information and power transfer. IEEE Globecom Workshops, pp. 1151–1156. 10.1109/GLOCOMW.2014.7063588.

XXIX. Tang, X., Alouini, M.-S. & Goldsmith, A.J., 1999. Effect of channel estimation error on M-QAM BER performance in Rayleigh fading. IEEE Transactions on Communications, 47, pp. 1856–1864. 10.1109/26.809706.

XXX. Trần, H.Q. & Van Khuong, H., 2024. Performance analysis for RIS-aided systems with energy harvesting. EAI Endorsed Transactions on Industrial Networks and Intelligent Systems, 11(1), e2. 10.4108/eetinis.v11i1.4369.

XXXI. Varshney, L.R., 2008. Transporting information and energy simultaneously. IEEE ISIT, pp. 1612–1616. 10.1109/ISIT.2008.4595260.

XXXII. Van, P.T. et al., 2016. Performance analysis in wireless power transfer system over Nakagami fading channels. ICEIC, pp. 1–4. 10.1109/ELINFOCOM.2016.75629718.

XXXIII. Yao, M. & Jin, J., 2007. Effect of channel estimation errors on MQAM with MRC and EGC. IEEE Transactions on Vehicular Technology, 56, pp. 1239–1250. 10.1109/TVT.2007.895491.

XXXIV. Yao, M., Schober, R. & Dongbo, Z., 2007. Exact BER for M-QAM with MRC and imperfect channel estimation. IEEE Transactions on Wireless Communications, 6, pp. 926–936. 10.1109/TWC.2007.05243.

XXXV. Zhou, X., Zhang, R. & Ho, C.K., 2013. Wireless information and power transfer: Architecture design and rate-energy tradeoff. IEEE Transactions on Communications, 61(11), pp. 4754–4767. 10.1109/TCOMM.2013.13.120855.

XXXVI. Zhu, P.Z. et al., 2022. Secrecy rate optimization in nonlinear energy harvesting model-based mmWave IoT systems. IEEE Systems Journal, 16(4), pp. 5939–5949. https://doi.org/10.1109/JSYST.2022.3147889.